The 9th European Congress on Computational Methods in Applied Sciences and Engineering
ECCOMAS Congress 2024
3–7 June 2024, Lisboa, Portugal

LEVEL-SET BASED COMPOSITE VOXELS FOR FFT-BASED COMPUTATIONAL HOMOGENIZATION OF THERMAL CONDUCTIVITY

JONAS LENDVAI[1] AND MATTI SCHNEIDER[1,2]

[1] University of Duisburg-Essen (UDE),
Institute of Engineering Mathematics,
45141 Essen, Germany

[2] Fraunhofer Institute for Industrial Mathematics ITWM,
Department Flow and Material Simulation,
67663 Kaiserslautern, Germany

Key words: Computational homogenization, FFT-based methods, Thermal conductivity problems, Composite voxel method

Summary. Computational homogenization methods reveal the physical behavior of heterogeneous materials, often complex due to intricate manufacturing. Micromechanical techniques use microstructural data to predict effective behavior. However, processing digital material data, represented as voxels, involves handling numerous image points. While modern FFT-based solvers are powerful, performance improvements remain beneficial. The composite voxel technique, in its original form, enhances accuracy by applying a surrogate material law to voxels containing more than one material phase. This work contributes to the understanding and application of composite voxels for thermal conductivity problems by integrating them into a level-set-based framework. Using FFT-based solvers, we demonstrate their potential to enhance computational performance through numerical examples.

1 INTRODUCTION

Computational homogenization methods offer valuable insights into the physical behavior of materials with heterogeneity at smaller scales. The complex anisotropic properties these materials develop, often as a result of intricate manufacturing processes, make experimental characterization both costly and time-consuming. However, micromechanical techniques utilize the material's microstructure as a blueprint, enabling the prediction of its effective behavior based on the phases and their spatial distribution.
In the most common applications, digital material data are typically represented as voxels (volume pixels), which results in the processing of a considerable number of image points. Due to the rectangular nature of voxels, interfaces between materials are often jagged, complicating the generation of high-quality and interface-conforming meshes. A more efficient approach is to work directly on the regular voxel grid, eliminating the need to store the mesh topology [1, 2].
In order to circumvent the difficulties associated with the generation of interface-conforming meshes, Moulinec-Suquet's [3, 4] approach employs regular, rectangular grids and solves periodic homogenization problems through the use of the fast Fourier transform (FFT) where efficient

implementations are available [5]. Since the original article, numerous novel insights, improvements and extensions have been presented, as thoroughly reviewed in recent articles [6, 7, 8]. These discoveries have been especially important in material science for addressing challenges related to mechanical and thermal conductivity.
While FFT-based methods are computationally powerful, there is still value in improving their performance. One significant advancement in this area is the composite voxel technique, independently developed by two research groups [9, 10] addressing mechanical problems, and also applied to thermal problems [11]. This approach involves representing the microstructure with greater detail than the voxel mesh used for the simulation. When the microstructure is provided analytically or as a high-resolution subvoxel image, certain voxels may include multiple phases. To capture this heterogeneity, these voxels are assigned a *composite* constitutive law. Various methods have been tested, and for materials with finite contrast, the most effective strategy is to apply a laminate constitutive law [12, §9], using accurate volume fractions and aligning the lamination direction close to the normal of the linear interface approximation within the composite voxel.
The article at hand contributes to the understanding and application of composite voxels for thermal homogenization problems, extending our recent work [13]. We shed light on whether the techniques developed for elasticity also provide accurate predictions for thermal conductivity. In Section 2, we provide a brief overview of the thermal conductivity problem that we are addressing. We reintroduce laminate voxels and their application to the thermal conductivity problem. We demonstrate how to calculate the effective conductivity of a laminate voxel and how to integrate laminate voxels into a level-set-based microstructure framework, see Section 3. Last, two numerical examples illustrate the potential of laminate composite voxels to enhance the computational performance, see Section 4 for details.

2 PERIODIC HOMOGENIZATION OF THERMAL CONDUCTIVITY

2.1 The thermal conductivity problem

Consider a rectangular domain $Y \subset \mathbb{R}^d$ with spatial dimension $d = 2, 3$. The objective is to extract an effective thermal conductivity tensor $\boldsymbol{\kappa}^{\text{eff}}$ of a microstructured material by solving the cell problem for a prescribed (negative) temperature gradient $\bar{\boldsymbol{\xi}}$. We assume that the local conductivity tensor

$$\boldsymbol{\kappa} : Y \to L(\mathrm{Sym}(d)), \tag{1}$$

given on the cell Y, is symmetric, bounded and uniformly positive definite. The set of linear mappings on the vector space V is denoted by $L(V)$ and $\mathrm{Sym}(d)$ refers to the space of symmetric $d \times d$ tensors. We aim to find a periodic temperature fluctuation field $\theta \in H^1_{\#}(Y; \mathbb{R}^d)$ with vanishing mean for a given macroscopic temperature gradient $\bar{\boldsymbol{\xi}} \in \mathrm{Sym}(d)$. The local negative temperature gradient is given by

$$\boldsymbol{\xi}(\boldsymbol{x}) = \bar{\boldsymbol{\xi}} - \nabla\theta(\boldsymbol{x}), \quad \boldsymbol{x} \in Y, \tag{2}$$

and the constitutive law follows Fourier's law

$$\boldsymbol{q}(\boldsymbol{x}) = \boldsymbol{\kappa}(\boldsymbol{x})[\boldsymbol{\xi}(\boldsymbol{x})], \quad \boldsymbol{x} \in Y. \tag{3}$$

The heat flux $\boldsymbol{q}$ has to fulfill the static heat equation

$$\operatorname{div} \boldsymbol{q}(\boldsymbol{x}) = 0, \tag{4}$$

leading to the cell problem

$$\operatorname{div} \left(\boldsymbol{\kappa}(\boldsymbol{x})[\, \bar{\boldsymbol{\xi}} - \nabla\theta(\boldsymbol{x})]\right) = 0. \tag{5}$$

We define the short-hand notation $\langle\cdot\rangle_Y = \frac{1}{|Y|}\int_Y \ \cdot \ d\boldsymbol{x}$ as the volume average of a field variable over the cell Y. With this notation at hand, the macroscopic temperature gradient satisfies $\bar{\boldsymbol{\xi}} = \langle\boldsymbol{\xi}\rangle_Y$. We define the effective heat flux as

$$\boldsymbol{q}^{\text{eff}}\left(\bar{\boldsymbol{\xi}}\right) := \langle\boldsymbol{q}\rangle_Y \tag{6}$$

It may be equivalently represented in the form

$$\boldsymbol{q}^{\text{eff}}\left(\bar{\boldsymbol{\xi}}\right) = \langle\boldsymbol{\kappa}\,[\boldsymbol{\xi}]\rangle_Y = \left\langle\boldsymbol{\kappa}\left[\, \bar{\boldsymbol{\xi}} - \nabla\theta\right]\right\rangle_Y. \tag{7}$$

Since Eq. (3) is linear, we implicitly define the effective conductivity tensor $\boldsymbol{\kappa}^{\text{eff}}$ via the effective constitutive law

$$\boldsymbol{q}^{\text{eff}}\left(\bar{\boldsymbol{\xi}}\right) = \boldsymbol{\kappa}^{\text{eff}}\left[\, \bar{\boldsymbol{\xi}}\, \right], \quad \bar{\boldsymbol{\xi}} \in \mathbb{R}^d. \tag{8}$$

Combining Eq. (7) and (8) leads to an implicit formula for the effective conductivity [14]

$$\boldsymbol{\kappa}^{\text{eff}}\left[\, \bar{\boldsymbol{\xi}}\, \right] = \left\langle\boldsymbol{\kappa}(\boldsymbol{x})\left[\, \bar{\boldsymbol{\xi}} - \nabla\theta(\boldsymbol{x})\right]\right\rangle_Y. \tag{9}$$

2.2 Lippmann-Schwinger formulation

The cell problem (5) may be reformulated as a fixed point equation by introducing a homogeneous reference conductivity $\boldsymbol{\kappa}_0 = \kappa_0\boldsymbol{I}$. We obtain the equivalent Lippmann-Schwinger equation [15, 16, 17, 18]

$$\boldsymbol{\xi} = \bar{\boldsymbol{\xi}} - \Gamma^0\,[\boldsymbol{\tau}] \quad \text{with the heat-flux polarization} \quad \boldsymbol{\tau} = (\boldsymbol{\kappa} - \boldsymbol{\kappa}_0)\,[\boldsymbol{\xi}], \tag{10}$$

and the local Eshelby-Green operator $\Gamma^0 = 1/\kappa_0\ \nabla\,(\operatorname{div}\nabla)^\dagger \operatorname{div}$, where $(\cdot)^\dagger$ refers to the Moore-Penrose pseudoinverse. Moulinec and Suquet [3, 4] developed an iterative scheme based on the fixed-point form of Eq. (10), initially for mechanical problems, known as the basic scheme. Their approach is applicable to thermal conductivity problems resulting in the iterative scheme given by

$$\boldsymbol{\xi}^{k+1} = \bar{\boldsymbol{\xi}} - \Gamma^0\left[\boldsymbol{\tau}^k\right] \quad \text{with} \quad \boldsymbol{\tau}^k = (\boldsymbol{\kappa} - \boldsymbol{\kappa}_0)\,[\boldsymbol{\xi}^k], \tag{11}$$

which can be interpreted as a preconditioned gradient descent scheme [19]. For any reference conductivity $\boldsymbol{\kappa}_0$ and initial temperature gradient $\boldsymbol{\xi}^0$, the basic scheme has a unique fixed point. The reference conductivity determines the convergence rate of the fix point scheme [20].
A crucial prerequisite for the efficiency of the basic scheme is the possibility to evaluate the Eshelby-Green operator Γ^0 with low computational effort. The FFT enables this task by facilitating its computation in Fourier space, leveraging highly efficient FFT implementations [5]. Recently, several research works [21, 22, 23] proposed strategies to impose non-periodic boundary conditions using the discrete sine and cosine transforms. We refer to the review articles [6, 7, 8] for details on error estimates, convergence behavior and alternative solving schemes for the iterative Lippmann-Schwinger equation (11), and a guidance on various discretization schemes.

3 COMPOSITE VOXELS IN COMPUTATIONAL HOMOGENIZATION

In this section, we discuss the composite voxel method, more precisely *laminate* composite voxels, known in the context of voxel-based micromechanics [9, 10, 24] and thermal conductivity problems [11]. Laminate materials [12, §9] are special microstructures which only vary in a particular direction. As illustrated in Fig. 1 for a two-phase microstructure, with an analytic representation of microstructure phases being available, there are heterogeneous voxel elements, i.e., elements comprising multiple microstructure phases, arising for any discretization on a regular grid. In their work, Kabel et al. [10] proposed to furnish those non-homogeneous voxels with the effective properties of an equivalent laminate. More precisely, the approach involves creating a microstructure layered in a direction approximating the interface normal and the appropriate cut volume fractions of each phase within the voxel.

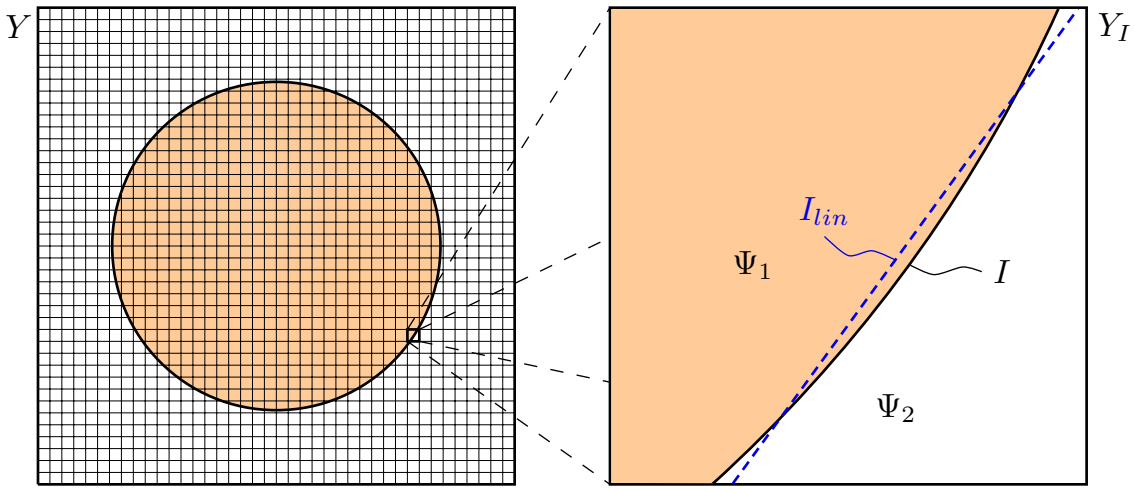

Figure 1: Illustration of a material microstructure with two phases $\Psi_{1,2}$ and an analytically given smooth interface I on a regular grid. A detailed view of a single interface voxel Y_I is presented on the right, including a potential linear interface approximation I_{lin}.

Originally part of *material modeling*, the composite voxel approach [10] kept the discrete kinematic compatibility and equilibrium equations unchanged but modified the constitutive law of composite voxels compared to homogeneous ones. Although laminate effective properties were initially used without a layering or periodicity of the "microstructure" within the voxel, recent research [13] demonstrated that laminate-type composite voxels can be justified by a kinematic assumption within a discretization scheme for micromechanical problems.
To obtain the effective properties of the equivalent laminate, we investigate the cell problem for a multiphased voxel. Let Y_I be a composite voxel cut by the material interface I, as illustrated on the right hand side of Fig. 1. Denote by

$$\phi_{1,2} = \operatorname{vol}(\Psi_{1,2}) \,/\, \operatorname{vol}(Y_I) \quad \text{with} \quad Y_I \equiv \overline{\Psi}_1 \cup \overline{\Psi}_2 \tag{12}$$

the volume fractions of the composite domains $\Psi_{1,2} \subseteq Y_I$. We further introduce a unit vector $\boldsymbol{n} \in \mathbb{R}^d$ representing the normal of a linear interface approximation I_{lin} between the phases $\Psi_{1,2}$ inside the composite voxel Y_I.

We are interested in finding the effective conductivity tensor $\boldsymbol{\kappa}_I^{\text{eff}}$ for this laminate voxel Y_I with an arbitrary direction of lamination $\boldsymbol{n}$ by solving the thermal conductivity problem Eq. (9). For a temperature gradient $\bar{\boldsymbol{\xi}}_I$, the problem reads

$$\boldsymbol{\kappa}_I^{\text{eff}} \left[\, \bar{\boldsymbol{\xi}}_I \, \right] = \left\langle \boldsymbol{\kappa}(\boldsymbol{x}) \left[\, \bar{\boldsymbol{\xi}}_I - \nabla \theta_I(\boldsymbol{x}) \right] \right\rangle_{Y_I} , \tag{13}$$

where $\boldsymbol{\kappa}_I(\boldsymbol{x})$ denotes the thermal conductivity of each phase within the laminate voxel. The local temperature gradient $\nabla \theta_I(\boldsymbol{x})$ is supposed to have a vanishing mean, allowing for a simplification of Eq. (13) to

$$\boldsymbol{\kappa}_I^{\text{eff}} \left[\, \bar{\boldsymbol{\xi}}_I \, \right] = \left\langle \boldsymbol{\kappa}(\boldsymbol{x}) \left[\, \bar{\boldsymbol{\xi}}_I \right] \right\rangle_{Y_I} . \tag{14}$$

Following Milton [12, §9], we introduce an orthogonal decomposition of the vector $\bar{\boldsymbol{\xi}}_I$ using the projectors

$$\boldsymbol{P}_1 = \boldsymbol{n} \otimes \boldsymbol{n}, \qquad \boldsymbol{P}_1 \boldsymbol{v} \in \{ \alpha \boldsymbol{n} \mid \alpha \in \mathbb{R} \} \quad \text{for any} \quad \boldsymbol{v} \in \mathbb{R}^d, \tag{15}$$

$$\boldsymbol{P}_2 = \boldsymbol{I} - \boldsymbol{n} \otimes \boldsymbol{n}, \qquad \boldsymbol{P}_2 \boldsymbol{v} \in \left\{ \boldsymbol{n} \cdot \boldsymbol{a} = 0 \mid \boldsymbol{a} \in \mathbb{R}^d \right\} \quad \text{for any} \quad \boldsymbol{v} \in \mathbb{R}^d, \tag{16}$$

in the form

$$\bar{\boldsymbol{\xi}}_I = \boldsymbol{P}_1 \left[\, \bar{\boldsymbol{\xi}}_I \, \right] + \boldsymbol{P}_2 \left[\, \bar{\boldsymbol{\xi}}_I \, \right] = \boldsymbol{n} \otimes \boldsymbol{n} \left[\, \bar{\boldsymbol{\xi}}_I \, \right] + (\boldsymbol{I} - \boldsymbol{n} \otimes \boldsymbol{n}) \left[\, \bar{\boldsymbol{\xi}}_I \, \right] . \tag{17}$$

This decomposition allows us to split Eq. (14) into two parts

$$\boldsymbol{\kappa}_I^{\text{eff}} \left[\, \bar{\boldsymbol{\xi}}_I \, \right] = \left\langle \boldsymbol{\kappa}(\boldsymbol{x}) \left[\boldsymbol{n} \otimes \boldsymbol{n} \right] \left[\, \bar{\boldsymbol{\xi}}_I \, \right] \right\rangle_{Y_I} + \left\langle \boldsymbol{\kappa}(\boldsymbol{x}) \left[\boldsymbol{I} - \boldsymbol{n} \otimes \boldsymbol{n} \right] \left[\, \bar{\boldsymbol{\xi}}_I \, \right] \right\rangle_{Y_I} , \tag{18}$$

which leads to

$$\boldsymbol{\kappa}_I^{\text{eff}} = \left\langle \boldsymbol{\kappa}(\boldsymbol{x}) \left[\boldsymbol{n} \otimes \boldsymbol{n} \right] \right\rangle_{Y_I} + \left\langle \boldsymbol{\kappa}(\boldsymbol{x}) \left[\boldsymbol{I} - \boldsymbol{n} \otimes \boldsymbol{n} \right] \right\rangle_{Y_I} . \tag{19}$$

As a consequence of the decomposition, we observe a decoupling of the conductivity in both the parallel and orthogonal directions with respect to the lamination direction $\boldsymbol{n}$.
With respect to Fig. 1, we specify Eq. (19) for a two-phase laminate and the isotropic conductivities $\boldsymbol{\kappa}_1 = \kappa_1 \boldsymbol{I}$ and $\boldsymbol{\kappa}_2 = \kappa_2 \boldsymbol{I}$.

$$\boldsymbol{\kappa}_I^{\text{eff}} = \frac{1}{\frac{\phi_1}{\kappa_1} + \frac{\phi_2}{\kappa_2}} \left(\boldsymbol{n} \otimes \boldsymbol{n} \right) + \left(\phi_1 \kappa_1 + \phi_2 \kappa_2 \right) \left(\boldsymbol{I} - \boldsymbol{n} \otimes \boldsymbol{n} \right) . \tag{20}$$

Therefore, the effective thermal conductivity tensor $\boldsymbol{\kappa}_I^{\text{eff}}$ for a laminate composite voxel is given by a relatively straightforward analytic expression. The tensor is determined solely by the material constants κ_1 and κ_2, and the geometric properties of the interface intersecting the voxel.
In the classical application of the composite voxel method [9, 10, 11, 25], a more refined subvoxel-based background mesh is utilized to facilitate the computation of the necessary quantities, specifically cut volume fractions and normals. In the work at hand, an alternative approach for the extraction of composite voxel properties, based on a level-set description of the material interface, is used. This method provides accurate volume fractions and normal vectors [13],

while also ensuring compatibility with digital images. The objective is to identify the optimal linear level-set function through a linear regression analysis of the intersection points between the interface and the voxel edges. The regression provides the approximated interface normal directly. The volume fraction of the emerging polyhedron is computed using an adaption of Mirtich's formulas [26] as described in Lendvai-Schneider [27]. We implemented a Newton method to determine the optimal level-set cutoff value to reach to analytically known targeted volume fractions of each phase up to a high accuracy.

4 NUMERICAL INVESTIGATIONS

4.1 Setup

In this section, we investigate and compare the numerical performance of laminate composite voxels for thermal conductivity problems. We integrated the composite voxels into an existing in-house FFT-based solver, developed in Python with Cython extensions and an OpenMP parallelization. Willot's discretization [28] was used and the linear conjugate gradient method [29] was employed to resolve the static heat equation up to a tolerance of 10^{-5} for the natural convergence criterion [8]. Periodic boundary conditions were applied. The simulations were performed on a workstation computer featuring two AMD EPYC 9354 with 32 physical cores each and a total of 1.12TB of RAM.
For all computations, we used an isotropic thermal conductivity of 1 $W/(m \cdot K)$ for the matrix material and 10 $W/(m \cdot K)$ for the inclusion material.

4.2 A spherical inclusion

As our first numerical example, we investigate the behavior of laminate composite voxels for a single spherical inclusion. Each cell contains one spherical inclusion with a diameter of $7/32\ \pi$ of the edge length, resulting in an inclusion volume fraction of approximately 17%, see Fig. 2.

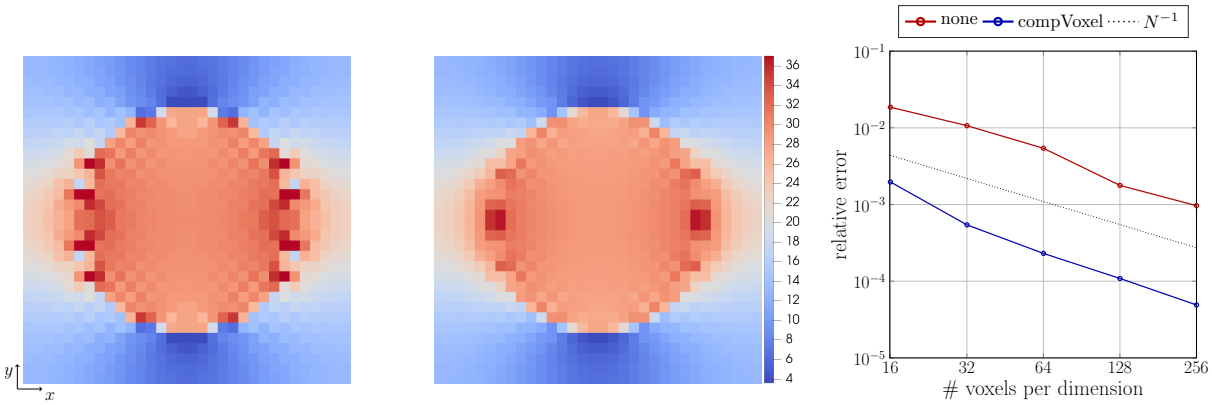

(a) 32^3 voxels, *none* (b) 32^3 voxels, *compVoxel* (c) Relative error vs. resolution

Figure 2: Influence of composite voxels on the heat flux magnitude for a single sphere inclusion in different resolutions. a), b): Comparison of the local heat flux magnitude $|\boldsymbol{q}|$ in W/m^2 on a resolution of 32^3 voxels without composite voxels (*none*) and with composite voxels (*compVoxel*). c): Relative errors of the computed effective heat flux $\boldsymbol{q}^{\text{eff}}$ in x-direction.

The diameter was chosen to be irrational to avoid pathological scenarios where the interfaces intersect the grid nodes frequently. We apply a temperature gradient of 10 K/m in x-direction as the boundary condition. With this setup at hand, we compare the local heat flux field with and without composite voxels for a resolution of 32^3 voxels. In Fig. 2a and 2b, the local heat flux magnitude $|\boldsymbol{q}|$ is shown. Using no composite voxels, we observe strong voxelization effects at the interfaces, in particular in the regions of very large and very small heat flux. Furthermore, there are strong checkerboarding artifacts [28]. As displayed in Fig. 2b, the use of composite voxels removes the voxelization effects to a large extent. Checkerboarding artifacts are less pronounced. This behavior is also observable in higher resolutions. All in all, we obtain a significantly improved solution quality.

We further investigate the effective material behavior under grid refinement by varying the resolution between 16 and 256 voxels per dimension. In Fig. 2c, the relative error in the x-component of the computed effective heat flux $\boldsymbol{q}^{\text{eff}}$ is shown. We use a numerical solution for 1024^3 voxels as our point of reference. For the simulations without composite voxels, we see that the relative error decreases from around 2% to 0.1% with increasing resolution. Using composite voxels lowers the relative error overall, reaching from 0.2% to below 0.01% for the finest resolution. The use of composite voxels lowers the relative error about one order of magnitude compared to the simulations without composite voxels.

4.3 A long fiber-reinforced composite structure

Last, we investigate the behavior of composite voxels for a long fiber-reinforced composite structure as an example of a material with random microstructure. Obtaining periodic microstructure images of long fiber-reinforced composites is challenging unless the microstructures are generated. With the fused sequential addition and migration algorithm [30], we are able to generate microstructures with long, curved fibers up to industrial volume fractions. We chose to generate a microstructure with an aspect ratio of 100 in a cubic unit cell with an edge length of 256μm. The dimensions of the fibers were considered to be 10μm in diameter and 1000μm in length, reinforcing a matrix at 21% volume fraction with 44 fibers. The fiber orientation was described by the second-order fiber-orientation tensor $\boldsymbol{A} = \text{diag}(0.77, 0.17, 0.06)$, utilizing the exact closure approximation [31, 32]. Consequently, the fibers wrap around the cell up to three times.

In order to prevent the formation of triple phase composite voxels, that is, voxels containing more than one intersecting fiber, the minimum inter-fiber distance was set to 7.2μm. This value was selected in consideration of the coarsest resolution of 64^3 voxels, where a fiber is resolved by 2.5 voxels in diameter. We followed the advice in Lauff et al. [30] and set the maximum segment length to 25μm, resulting in a maximum of 40 segments per fiber, and the maximum bending angle between the segments to 60°. A view on the generated microstructure is provided in Fig. 3a.

We construct the effective heat conductivity tensor $\boldsymbol{\kappa}^{\text{eff}}$ using Eq. (9) and applying three linearly independent load scenarios. As no analytical solution for the effective properties is available for this microstructure, we use a high-fidelity computation on 1024^3 voxels as our reference solution. The relative error is calculated using the Frobenius norm. The results of a resolution study using the composite voxel strategy are shown in Fig. 3b and compared to using only plain, i.e., no composite, voxels. We observe a decrease in the relative error from around

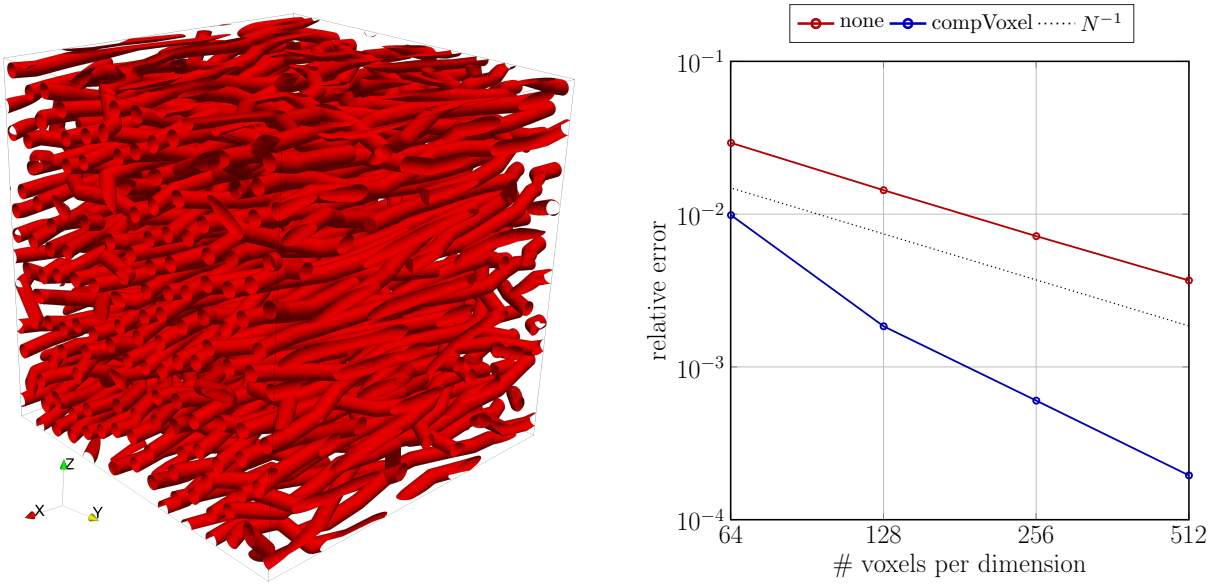

(a) 256^3 voxels

(b) Relative error vs. resolution

Figure 3: Influence of composite voxels on the effective thermal behavior of a long-fiber reinforced microstructure. a): View on the generated structure resolved by 256 voxels per dimension. b): Relative errors of the computed effective conductivity tensor for different resolutions.

3% to 0.5% with increasing resolution without using composite voxels. Using composite voxels lowers the relative error overall, reaching from 1% to below 0.02% for the finest resolution. The advantage is about one order of magnitude which roughly amounts to using only one fourth of the resolution per dimension required for a specific accuracy and avoiding the use of composite voxels. On the finest resolution, only 6.04% of the voxels are composite voxels compared to 50.51% for the microstructure resolved by 64^3 voxels. The use of composite voxels results in an about 20% increase in computational effort, independent of the resolution. This increase represents an excellent compromise given the savings in total resolution.

5 CONCLUSIONS

The work at hand was devoted to understanding using level-set based laminate composite voxels in the setting of FFT-based computational homogenization of thermal conductivity. Consequently, the problem setting of thermal conductivity was reintroduced, and a preliminary overview of the FFT-based homogenization regarding thermal conductivity problems was presented. We derived a possible integration of composite voxels into a level-set-based microstructure description utilizing Milton's [12] lamination rule and incorporating the precise computation of composite voxel properties. We demonstrated the advantages of the proposed method through two numerical examples, specifically a single sphere inclusion and a long-fiber reinforced composite microstructure. Our findings consistently identified an improvement in the quality of the computed effective properties, thereby offering the potential for a significant reduction in the required computational effort.

Acknowledgements

The support of the European Research Council through the Horizon Europe program -project 101040238- is gratefully acknowledged by MS. JL acknowledges the funding by the Deutsche Forschungsgemeinschaft (DFG, German Research Foundation) - 440998847-.

Data availability statement

The data that support the findings of this study are available from the corresponding author upon reasonable request.

REFERENCES

[1] J. M. Guedes and N. Kikuchi, "Preprocessing and postprocessing for materials based on the homogenization method with adaptive finite element methods," *Computer Methods in Applied Mechanics and Engineering*, vol. 83, no. 2, pp. 143–198, 1990.

[2] G. Nagai, T. Yamada, and A. Wada, "Finite element analysis of concrete material based on the 3-dimensional real image data," in *Computational Mechanics - New Trends and Applications* (S. Idelson, E. Oñate, and E. Dvorkin, eds.), vol. 1066, (Barcelona), pp. 1–14, CIMNE, 1998.

[3] H. Moulinec and P. Suquet, "A fast numerical method for computing the linear and nonlinear mechanical properties of composites," *Comptes Rendus de l'Académie des Sciences. Série II*, vol. 318, no. 11, pp. 1417–1423, 1994.

[4] H. Moulinec and P. Suquet, "A numerical method for computing the overall response of nonlinear composites with complex microstructure," *Computer Methods in Applied Mechanics and Engineering*, vol. 157, pp. 69–94, 1998.

[5] M. Frigo and S. G. Johnson, "The Design and Implementation of FFTW3," in *Proceedings of the IEEE*, vol. 93, pp. 216–231, 2005.

[6] R. A. Lebensohn and A. D. Rollett, "Spectral methods for full-field micromechanical modelling of polycrystalline material," *Computational Materials Science*, vol. 173, p. 109336, 2020.

[7] J. Segurado, R. A. Lebensohn, and J. LLorca, "Chapter One - Computational Homogenization of Polycrystals," *Advances in Applied Mechanics*, vol. 51, pp. 1–114, 2018.

[8] M. Schneider, "A review of non-linear FFT-based computational homogenization methods," *Acta Mechanica*, vol. 232, pp. 2051–2100, 2021.

[9] L. Gélébart and F. Ouaki, "Filtering material properties to improve FFT-based methods for numerical homogenization," *Journal of Computational Physics*, vol. 294, pp. 90–95, 2015.

[10] M. Kabel, D. Merkert, and M. Schneider, "Use of composite voxels in FFT-based homogenization," *Computer Methods in Applied Mechanics and Engineering*, vol. 294, pp. 168–188, 2015.

[11] D. Merkert, H. Andrä, M. Kabel, M. Schneider, and B. Simeon, *An efficient algorithm to include sub-voxel data in FFT-based homogenization for heat conductivity*, pp. 267–279. Cham: Springer, 2015.

[12] G. W. Milton, *The Theory of Composites*. Cambridge: Cambridge University Press, 2002.

[13] J. Lendvai and M. Schneider, "Assumed strain methods in micromechanics, laminate composite voxels and level sets," *International Journal for Numerical Methods in Engineering*, vol. 125, no. 11, p. e7459, 2024.

[14] C. Dorn and M. Schneider, "Lippmann-schwinger solvers for the explicit jump discretization for thermal computational homogenization problems," *International Journal for Numerical Methods in Engineering*, vol. 118, pp. 631–653, Mar. 2019.

[15] R. Zeller and P. H. Dederichs, "Elastic constants of polycrystals," *physica status solidi*, vol. 55, no. 2, pp. 831–842, 1973.

[16] E. Kröner, "Bounds for effective elastic moduli of disordered materials," *Journal of the Mechanics and Physics of Solids*, vol. 25, no. 2, pp. 137–155, 1977.

[17] T. Mura, *Micromechanics of Defects in Solids*. Dordrecht: Martinus Nijhoff, 1987.

[18] G. Vainikko, "Fast solvers of the lippmann-schwinger equation," *Direct and Inverse Problems of Mathematical Physics, International Society for Analysis Applications and Computation*, vol. 5, pp. 423–440, 2000.

[19] M. Kabel, T. Böhlke, and M. Schneider, "Efficient fixed point and Newton-Krylov solvers for FFT-based homogenization of elasticity at large deformations," *Computational Mechanics*, vol. 54, no. 6, pp. 1497–1514, 2014.

[20] D. J. Eyre and G. W. Milton, "A fast numerical scheme for computing the response of composites using grid refinement," *The European Physical Journal - Applied Physics*, vol. 6, no. 1, pp. 41–47, 1999.

[21] L. Risthaus and M. Schneider, "Imposing different boundary conditions for thermal computational homogenization problems with fft- and tensor-train-based green's operator methods," *International Journal for Numerical Methods in Engineering*, vol. 125, no. 7, p. e7423, 2024.

[22] L. Gélébart, "FFT-based simulations of heterogeneous conducting materials with combined non-uniform Neumann, periodic and Dirichlet boundary conditions," *European Journal of Mechanics - A/Solids*, p. 105248, 2024.

[23] L. Morin and J. Paux, "A fast numerical method for the conductivity of heterogeneous media with dirichlet boundary conditions based on discrete sine–cosine transforms," *Computer Methods in Applied Mechanics and Engineering*, vol. 421, p. 116772, 2024.

[24] M. Kabel, A. Fink, and M. Schneider, "The composite voxel technique for inelastic problems," *Computer Methods in Applied Mechanics and Engineering*, vol. 322, pp. 396–418, 2017.

[25] S. Keshav, F. Fritzen, and M. Kabel, "FFT-based homogenization at finite strains using composite boxels (ComBo)," *Computational Mechanics*, vol. 71, pp. 191–212, 2022.

[26] B. Mirtich, "Fast and accurate computation of polyhedral mass properties," *Journal of Graphics Tools*, vol. 1, no. 2, pp. 31–50, 1996.

[27] J. Lendvai and M. Schneider, "Computing laminate composite voxel properties using Mirtich formulas," *(submitted)*, pp. 1–9, 2024.

[28] F. Willot, "Fourier-based schemes for computing the mechanical response of composites with accurate local fields," *Comptes Rendus Mécanique*, vol. 343, pp. 232–245, 2015.

[29] J. Zeman, J. Vondřejc, J. Novák, and I. Marek, "Accelerating a FFT-based solver for numerical homogenization of periodic media by conjugate gradients," *Journal of Computational Physics*, vol. 229, no. 21, pp. 8065–8071, 2010.

[30] C. Lauff, M. Schneider, J. Montesano, and T. Böhlke, "Generating microstructures of long fiber reinforced composites by the fused sequential addition and migration method," *International Journal for Numerical Methods in Engineering*, p. e7573, 2024.

[31] S. Montgomery-Smith, W. He, D. Jack, and D. Smith, "Exact tensor closures for the three-dimensional Jeffery's equation," *Journal of Fluid Mechanics*, vol. 680, pp. 321–335, 2011.

[32] S. Montgomery-Smith, D. Jack, and D. E. Smith, "The Fast Exact Closure for Jeffery's equation with diffusion," *Journal of Non-Newtonian Fluid Mechanics*, vol. 166, pp. 343–353, 2011.